# Soy Protein Derived Thermoset Resins for Traditional Molding and 3-D Printing

Long Jiang, Qian Ma

ABSTRACT: Plastic wastes pose a serious threat to the environment and there have been strong interests in developing soy protein isolate (SPI) based plastics to reduce the use of traditional petroleum-based ones. However, the use of SPI plastics has been hindered due to their inferior mechanical properties and poor water resistance compared with traditional plastics. In this work, SPI plastics with significantly improved mechanical properties and water resistance were developed using UV curable SPI resin and UV curable cellulose nanofibers. Three UV curable materials, i.e. methacrylated SPI (MSPI), methacrylated cellulose nanofibrils (MCNF), and methacrylated cellulose nanocrystals (MCNC), were produced through methacrylation of SPI, CNF, and CNC, respectively. Methacrylation of the materials and UV curing of the resins was confirmed using Fourier-transform infrared spectroscopy. Uniform dispersion of CNC, CNF, MCNC, or MCNF in the resin was confirmed by scanning electron microscope and X-ray diffraction. Tensile properties and water resistance of the resins were found to improve with increasing curing time and degree of methacrylation. The incorporation of CNC, CNF, MCNC, and MCNF further improved the mechanical and water resistance performance of the resins, with the MCNF leading to the largest improvement. UV curing and the cellulose nanofibers evidently worked synergistically to improve the properties of the resins. This study demonstrated a method and formulations to produce SPI plastics with exceptional properties. Furthermore, the potential of this resin in 3D printing and conventional plastics molding was demonstrated.

KEYWORDS: Soy protein isolate (SPI), soy based plastics, cellulose nanofibrils (CNF), cellulose nanocrystals (CNCs), UV curing, 3D printing, nanocomposites, methacrylation.

## INTRODUCTION

Many methods have been studied and used to mitigate the severe environmental consequences of the widespread use of petroleum-based polymers. Replacing the petroleum-based polymers with naturally occurring biopolymers has shown great potential in many applications and has become an effective method to reduce the environmental impact of the plastic industry.[1,2] The use of biopolymers derived from biomass also adds value to many agricultural and forest byproducts and thus can provide important economic benefits to the respective industries. Many biopolymers such as proteins (soy protein, wheat gluten, whey, collagen, gelatin, etc.), polysaccharides (cellulose, starch, alginate, gum, chitosan, etc.), lipids (fats, oils, etc. ), or the combination of these components have been investigated as materials that can offer competitive properties, especially in their modified forms.[3–6] Among these biomaterials, proteins are a favorite source for developing biodegradable plastics because many of the nonpolar, polar, and charged groups in the protein chains provide functional sites for chemical modifications, which can lead to improved material properties or new material functions.[7,8]

Soy protein isolate (SPI), as a common soy protein material and a byproduct from the soybean oil industry, contains a minimum of 90% protein and consists of 18 different amino acids. Owing to its good film-forming ability, low cost, and desirable transparency, SPI has attracted considerable research interest in bioplastics application.[9] However, some fundamental limitations of SPI, such as poor processability and flexibility, insufficient mechanical strength, and low water resistance, have prevented it from widespread utilization. The limitations arise from strong intra- and intermolecular interactions among protein chains and the hydrophilic functional groups on the macromolecules.[10,11] To overcome these problems, many different physical or chemical modification methods, such as heating, microwaving, ultrasonic treatment, pH adjustment,

hydrolysis, blending, grafting, cross-linking, or incorporation of nano-reinforcements have been attempted to alter its native globular protein structure.

Heating, microwaving, and ultrasonic treatment have been utilized to produce SPI films with higher mechanical strength and hydrophobicity, since the use of a higher processing temperature can cause a higher degree of protein unfolding and denaturation.[12,13] It has been reported that hydrolysis or treatment of SPI at pH 11 or higher can lead to SPI adhesives or films with improved mechanical property and water resistance due to increased protein solubility.[14–16] SPI has been blended with hydrophobic thermoplastics (e.g. polylactic acid and polybutylene adipate-co-terephthalate) and fatty acid and lipids (e.g. oleic/steric acids, epoxidized soybean oil and olive oil) for enhanced performance due to stress transfer and reduced ratio of hydrophilic moieties.[17–20] However, good interactions and compatibility between the components is hard to achieve. Low-molecular-weight plasticizers such as glycerol, ethylene glycol, and propylene glycol have often been incorporated into SPI to improve its processability and flexibility. The plasticizing effect of plasticizers comes from their ability to position themselves within the three-dimensional protein network, increasing the free-volume and facilitating the mobility of the polymer chains.[21] However, these attempts to improve one specific property of SPI often lead to decreases in other properties.[22] Grafting new functional groups onto soy protein chains is another method to improve the performance of SPI plastics or to expand their functions. Various chemical agents have been employed to modify SPI for improving or adding new properties such as solubility and surface hydrophobicity.[23–27] Nevertheless, in spite of many physical and chemical modifications attempted on SPI, its drawbacks, such as low mechanical strength and poor water-resistance, still pose significant challenges for many applications.

Crosslinking is an effective approach to develop protein-based plastics with improved mechanical strength and water resistance because it creates intermolecular chemical bonding, increases molecular packing, and reduces polymer chain mobility, thus improving the overall properties of the material.[7] Proteins can be crosslinked thermally, enzymatically, chemically, or through photopolymerization.[15,28] Many of these methods involve either the use of toxic crosslinking agents or a considerable amount of time and energy for polymer network formation. Photopolymerization, also known as photo-crosslinking or UV curing, is a process that transforms multifunctional monomers into a crosslinked polymer network through a chain reaction initiated by free radicals, which are produced by an added photo-initiator under UV irradiation. The major advantages of photo-crosslinking over traditional crosslinking methods include low equipment costs, low energy consumption, short crosslinking time, low environmental impact, and excellent mechanical properties.

The incorporation of nanofillers is another promising method to obtain protein-based plastics with significantly improved properties. The incorporated nanoparticles can reinforce the matrix material by sharing its load and toughen the material by bridging and deflecting cracks.[29] A number of organic nanofillers (e.g. cellulose nanofibrils or nanocrystals and nanocrystals derived from zein, chitosan, and starch) and inorganic nanofillers (e.g. layered silicates, zinc oxide, titanium dioxide, silver, and carbon nanotubes) have been investigated as nano reinforcements to enhance the properties of numerous biopolymers.[7,21] It is well established that the effect of reinforcement depends primarily on the state of dispersion of the nanoparticles and the polymer-particle interactions.

As the most abundant biopolymer in the world, cellulose can be processed into nanofillers with a diverse morphology: from individually separated short cellulose nanocrystals (CNC) to long

cellulose nanofibrils (CNF) with a high aspect ratio and varied degrees of entanglement.[30] Nanocellulose is an effective reinforcement material because of its superior mechanical properties, high aspect ratio, and the availability of many modification methods to tailor its surface.[31,32] CNF can be produced by a mechanical fibrillation process with or without prior chemical treatments, which creates long, flexible, and often entangled cellulose nanofibrils with a diameter between 20 and 60 nm.[33–35] CNC is obtained through acid hydrolysis of cellulosic fibrils and is a rigid, rod-like crystal between 3 and 20 nm in width and a few hundred nanometers in length.[36,37] It has been shown that the incorporation of even a low concentration of uniformly-dispersed CNF or CNC in a polymeric matrix can lead to a significant improvement in its mechanical properties.[29] Unfortunately, it is still challenging to reinforce hydrophobic polymers using CNF or CNC because of weak CNF/CNC-polymer interfacial bonding and poor CNF/CNC dispersion in the polymer matrixes.[38] Additionally, the strong hydrophilic nature of cellulose leads to poor water resistance of the products and thus hinders its use in plastic applications.[39,40] However, the hydrophilicity of nanocellulose can be decreased and its compatibility with the polymer matrixes can be improved by chemically modifying its surface. Many studies have been reported on nanocellulose surface modifications through reacting with its hydroxyl groups using various reagents including mineral and organic acids, bases, oxidizing agents, and organic compounds.[30,41]

Cellulose has also been used to reinforce SPI based plastics. Zhang et al. compared the effects of pristine and surface-modified cellulose nanocrystals on the properties of SPI films. Compared with the pristine CNC, the modified CNC resulted in significantly higher strength, stronger water resistance, and higher thermal stability due to the crosslinking between SPI and the modified CNC.[42] Zheng et al. prepared SPI/dialdehyde carboxymethyl cellulose (DCMC) composite films and studied the effect of DCMC on the mechanical properties, water sensitivity, light barrier

properties and thermal stability of the composite films.[43] Kang et al. modified the surface of microcrystalline cellulose (MCC) by simply dip-coating it with dopamine and then prepared SPI/polydopamine (PDA)-modified MCC composite films. They reported that the modification enhanced the interfacial adhesion between MCC and SPI and thus greatly enhanced the mechanical properties and reduced water absorption of the resultant films.[44]

Despite several reported research studies on soy protein plastic reinforcement using cellulose nanofibers in the literature, to the best of our knowledge, combining the method of cellulose nano reinforcement with the method of soy protein UV crosslinking for further property improvements of the soy plastics has not yet been attempted. The goal of this study is to explore the synergy between these two methods through synthesizing UV curable CNC/CNF and SPI to produce soy protein plastics with properties that cannot be achieved by using either of the methods alone. This study provides a facile, effective strategy to improve the performance of SPI plastics and facilitate SPI utilization.

## EXPERIMENTAL SECTION

**Materials.** Soy protein isolate (SPI) (PRO-FAM® 974) was supplied by Archer Daniels Midland Company. CNF slurry and CNC suspension were purchased from the Process Development Plant of University of Maine. Potassium Hydroxide (KOH) (85%) and 2-Hydroxy-2-methylpropiophenone (≥ 96.0%) were purchased from Fisher Scientific. Methacrylic anhydride (MAh) (94%) and sodium hydroxide (⩾ 98.0%) were purchased from Sigma-Aldrich. All the chemicals were used as received without further purification.

**Synthesis of Methacrylated SPI (MSPI).** The synthesis of MSPI was performed though a two-step process including SPI dissolution and SPI methacrylation based on a previously reported study.[45] Briefly, SPI was mixed with distilled water (15 wt%) in a round bottom flask. A KOH

aqueous solution (8 wt%) was added to the SPI/water mixture in the flask to give a SPI/$H_2O$/KOH ratio of 1/7/0.09 (w/w/w) and a pH value of 11.6. The flask was then placed in a preheated oil bath at 70 $^oC$ and the mixture was magnetically stirred at 450 rpm for 1.5 h to complete the dissolution. The product was allowed to cool to room temperature naturally for about 30min and centrifuged at 9000 rpm for 5 min to remove any undissolved SPI and impurities. In the second step, the alkali-treated SPI was reacted with methacrylic anhydride (MAh) to synthesize MSPI. MAh (6, 10, or 14 wt% of SPI dry weight) was added into the SPI solution and stirred with a magnetic stirrer (500 rpm) at room temperature for 30 min to obtain MSPI with different degrees of methacrylation.

**Synthesis of Methacrylated Nanocellulose (MCNF and MCNC).** MCNF and MCNC were synthesized by reacting CNF or CNC with methacrylic anhydride (MAh) at 50 $^oC$ for 4 h.[46] Briefly, 4 g (dry weight) of CNF or CNC were dispersed in 400 ml of deionized water using an IKA RW20 digital homogenizer (656 rpm) for 30 min at room temperature. The temperature of the colloidal suspension was increased to 50 °C and 40 g MAh was added. The reaction was continued for 4 h while the pH of the suspension was maintained at 8-10 by adding 5 N NaOH solution. The resulting suspension was washed with deionized water by repeated centrifugations (11000 rpm, 5 min per cycle) until the pH was 7.

**Preparation of MSPI Composite Films.** MSPI solution, CNF, MCNF, CNC, or MCNC (10 wt% MSPI), plasticizer (glycerol, 50 wt% MSPI), and photo-initiator (PI) (2-Hydroxy-2-methylpropiophenone) (8 wt% methacrylated macromer) were mixed together using an IKA T25 digital ultra-turrax homogenizer (3400 rpm) for 30 min at room temperature. The mixture (pH 7.7) was poured into a polypropylene Petri dish and allowed to dry under ambient conditions for 2 days. The obtained film (thickness ~ 0.4 mm) was then crosslinked under a UV lamp (365 nm/250 W, 20 cm distance between the lap and the sample).

**Sample Characterization.** Chemical bonds of MSPI, MCNF, and MSPI films after different UV curing times were characterized using Fourier-transform infrared spectroscopy (FTIR). The analysis was carried out on a Thermo Scientific Nicolet 8700 FTIR Spectrometer (Waltham, MA) equipped with an ATR probe (4 $cm^{-1}$ resolution and 32 repeated scans). To prepare MSPI for the FTIR analysis, the MSPI solution was dialyzed using dialysis tubing (MWCO=3500) against deionized water for 72h to remove any residual reagents and contaminates. The dialyzed MSPI solution was dried, ground into powder, and mixed with KBr for the analysis. The spectra were collected over the wavenumber range of 4000-400 $cm^{-1}$. To characterize MCNF, the methacrylated CNF suspension was dried in a vacuum oven into a thin film and its FTIR spectra were collected using the ATR accessory (4000-650 $cm^{-1}$). All the composite film samples were also characterized using the same ATR technique.

Tensile properties of the composite films were studied using an Instron 5545 mechanical tester equipped with a 100 N load cell. The films were cut into 1 cm × 5 cm strips and tested with a gauge length of 3 cm and a crosshead speed of 50 mm/min. For wet sample testing, the samples were taken out of the water after 8 hours of immersion and dabbed dry with a paper towel before the tests.

The morphology of the composite films (surfaces and cross-sections) was studied using a field-emission scanning electron microscope (SEM, JSM-7600F, JEOL, Japan) at an accelerating voltage of 2 kV. The cross-sections were obtained by freezing and fracturing the films in liquid nitrogen. The specimens were coated with a thin layer of gold before imaging.

X-ray diffraction (XRD) measurements were carried out using a D8 Discover X-ray diffractometer (Bruker, Karlsruhe, Germany) with Cu Kα radiation (λ=0.154 nm) at 40 kV and 40 mA at a rate of 2º/min. The 2θ range was 5-60º. Samples were prepared by fixing 2 cm × 3 cm

sample films flat on top of a glass slide using tapes. Crystallinity index (CI) of the samples was determined based on the XRD diffraction patterns using the following equation [47,48]:

$$CI(\%) = \frac{I_{cr} - I_{am}}{I_{cr}} \times 100 \quad (1)$$

where $I_{cr}$ is the intensity of the main diffraction peak of the samples (at 20.04º or 21.25º) and $I_{am}$ is the diffraction intensity of the amorphous fraction of the samples (sampled at 12.78 º).

## RESULTS AND DISCUSSION

**Synthesis and Characterization of Macromers.** Figures 1a and 1b show the simplified reaction schemes for methacrylation of SPI, CNF, and CNC. Methacrylate groups are grafted onto the three materials through methacrylic anhydride's reactions with the amine or hydroxyl groups. Figure 1c illustrates the UV curing mechanism for MSPI and MCNF (or MCNC) to produce crosslinked SPI films. Under UV irradiation, free radicals generated from the added photo-initiator attack the C=C bonds of the grafted methacrylate groups and induce crosslinking between these groups, eventually leading to an interpenetrated network structure.

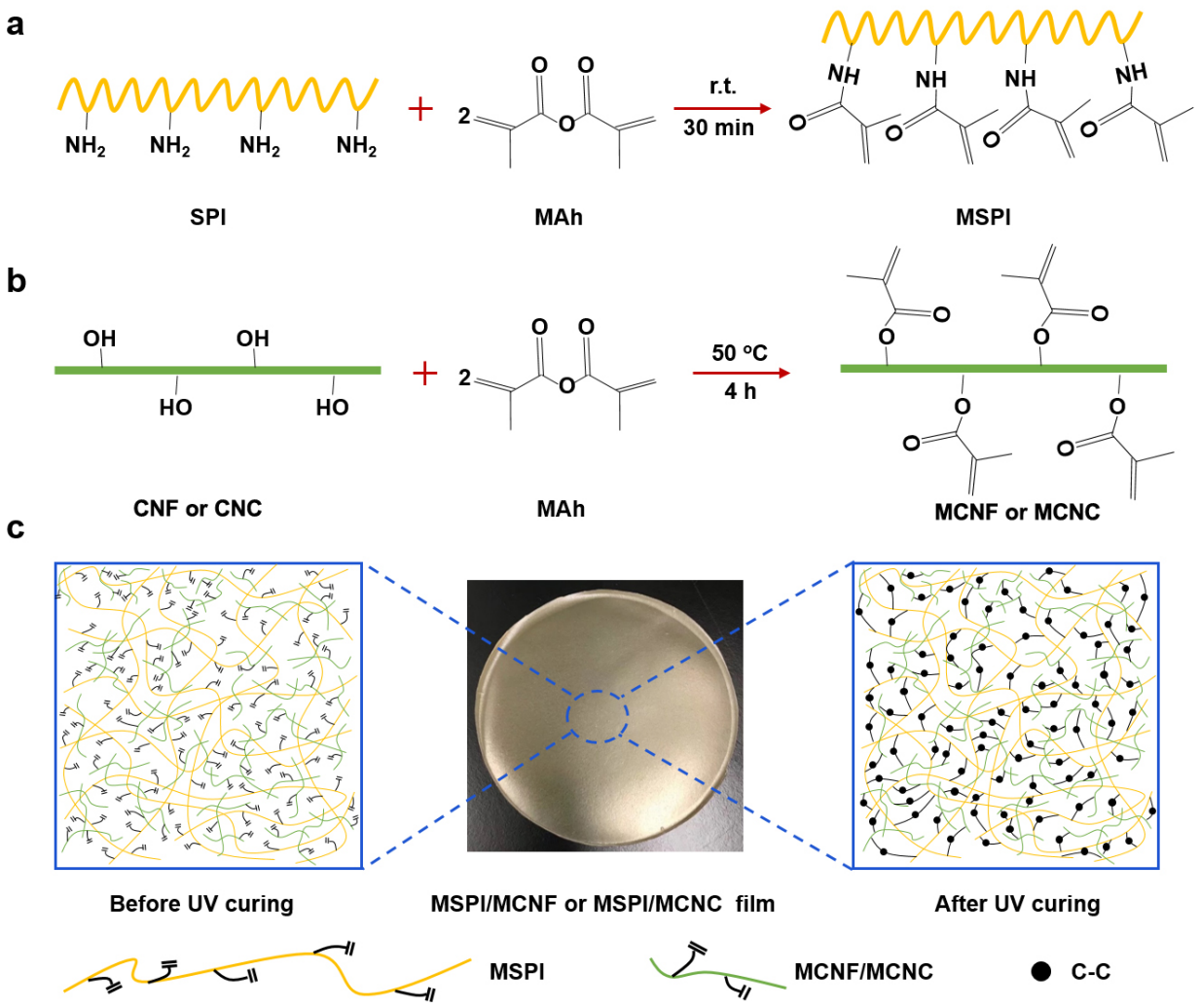


**Figure 1.** Simplified reaction schemes for the MSPI (a) and MCNF or MCNC (b) synthesis, and the mechanism of MSPI/MCNF and MSPI/MCNC crosslinking under UV irradiation (c).

Methacrylation of SPI and CNF was confirmed using FTIR. In Figure 2a, alkaline treated SPI showed characteristic amide bands at 1657, 1527, 1391, and 1231 $cm^{-1}$ assigned to amide I (C=O stretching), amide II (N–H bending), and amide III (C–N and N–H stretching), respectively.[49,50] After the methacrylation, two new peaks appeared in all the MSPI samples at 1130 $cm^{-1}$ and 930 $cm^{-1}$ (representing wagging and stretching of C-H of $RC=CH_2$, respectively).[51,52] The signal from C=C of the methacrylate group was difficult to detect because it overlapped with the signature

from the amide I of SPI. Meanwhile, peaks at 1316 $cm^{-1}$ and 1169 $cm^{-1}$ of all the MSPI samples became stronger than that of alkaline treated SPI due to C-$CH_3$ stretching and C-O stretching of the methacrylate group, respectively.[53,54] These results indicated successful grafting of the methacrylate group onto SPI. The FTIR spectra of CNF and MCNF are compared in Figure 2b. Characteristic absorption peaks of CNF were observed at around 3329 $cm^{-1}$ (O-H stretching), 2919, and 2849 $cm^{-1}$ (both for C-H stretching of $CH_2$). Other major peaks detected included the absorption bands at 1645 $cm^{-1}$ (bound water), 1368 $cm^{-1}$ (C-H bending), 1161 $cm^{-1}$ (C-O-C stretching), 1106 $cm^{-1}$ (C-O stretching), and 1055 $cm^{-1}$ (C-O and C-C stretching).[38,55] After the methacrylation, three new peaks at 1720 $cm^{-1}$ (C=O stretching), 1635 $cm^{-1}$ (C=C vibration), and 1551 $cm^{-1}$ (C=O stretching of CH=CHCOO–$Na^+$) appeared on the spectrum of MCNF.[56] The peak at 1368 $cm^{-1}$ of MCNF also became stronger than that of CNF due to C-$CH_3$ stretching. These results confirmed the successful methacrylation of CNF.[54]

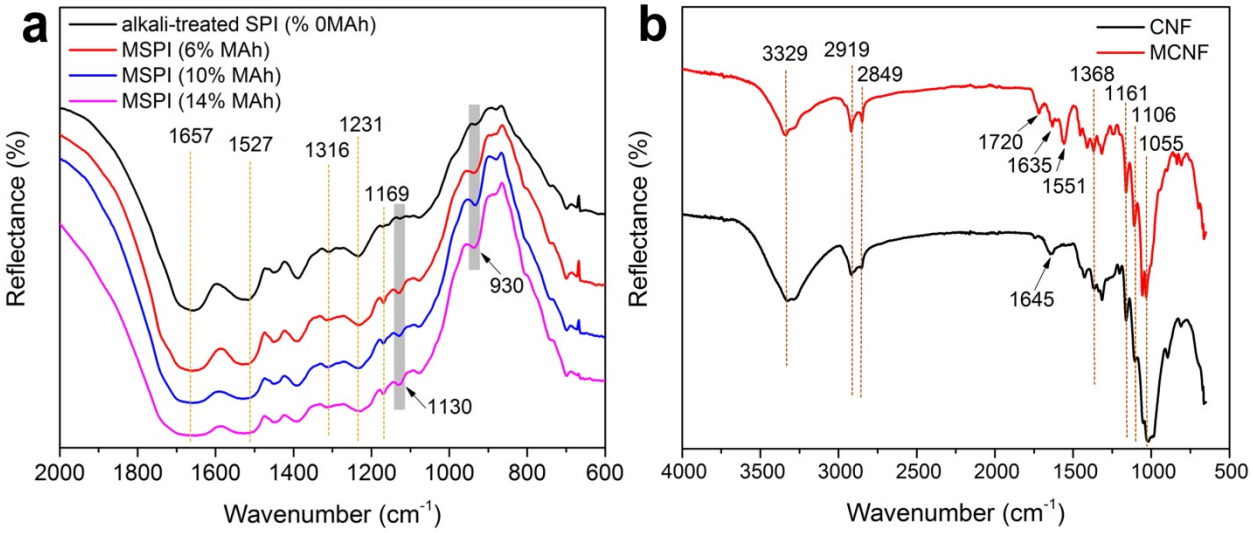


**Figure 2.** FTIR spectra of alkali-treated SPI and MSPI (a) and pristine CNF and MCNF (b).

**UV Crosslinking of MSPI.** UV crosslinking of MSPI was confirmed by the consumption of C=C bonds during the reaction and the increased mechanical properties of the MSPI films after

UV irradiation. Figure 3a compares the FTIR spectra of MSPI films cured for different amounts of time. The region between 1650 and 1625 $cm^{-1}$ is attributed to the vibrations from both amide I of SPI and C=C of the methacrylate. A lower intensity of this region was noted with a longer curing time (the spectra were increasingly flattened). Because amide I was not involved in the curing reaction, the flattening of the spectra indicates the cleavage/consumption of C=C bonds during the free radical polymerization.[46,57]

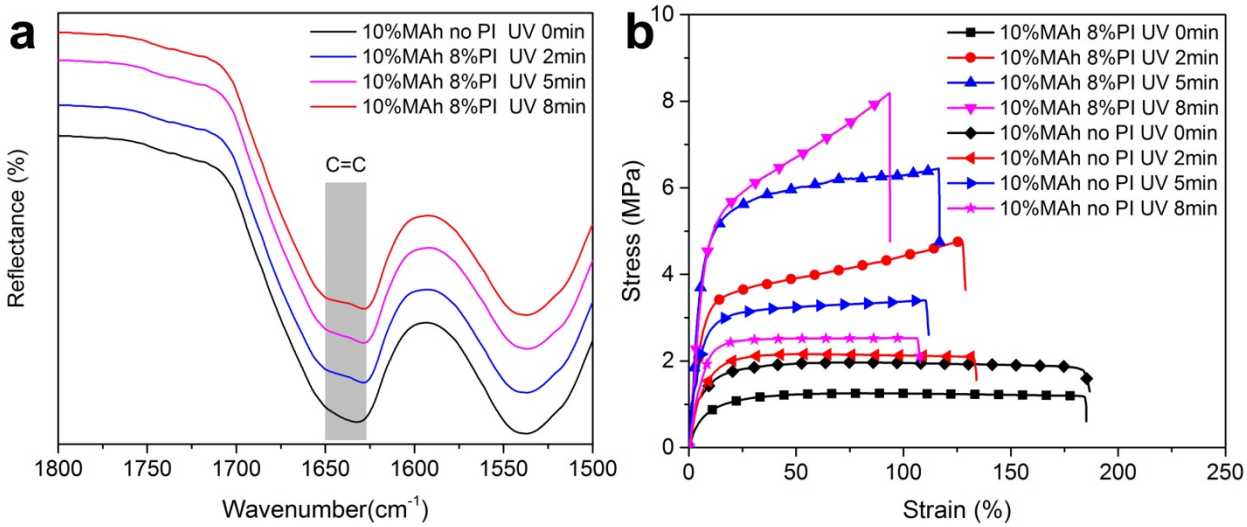


**Figure 3.** FTIR spectra (a) and stress-strain curves (b) of MSPI films (methacrylated with 10 wt% MAh) after UV curing for various minutes. The films contained either no PI or 8 wt% PI for initiating UV crosslinking.

Figure 3b shows the tensile stress-strain curves of the MSPI films. The tensile properties of the films were calculated based on the curves and the results are summarized in Table S1. The sample not subjected to UV irradiation, i.e. sample "10%MAh 8%PI UV 0min", showed the lowest failure stress and modulus and the highest failure strain among all the films, indicating that the sample was a weak and flexible material without UV curing. The fracture stresses and moduli of all the films, regardless of the presence of PI, increased with the increasing curing time. For the films

containing PI, the stress and modulus increased from 1.22 MPa and 16.23 MPa at 0 min UV irradiation to 8.39 MPa and 74.25 MPa at 8 min UV irradiation, respectively. For the films containing no PI, the stress and modulus increased from 1.97 MPa and 29.17 MPa to 2.59 MPa and 37.56 MPa, respectively, under the same conditions. The samples containing PI showed much larger property increases than the samples without PI because of the former's crosslinked molecular structures caused by the UV crosslinking.[58] The samples containing no PI were not able to undergo UV curing due to their lack of PI. However, the heat from the UV lamp during the curing process caused temperature increases of the films, which led to heat-induced protein denaturization and thus mild improvements in sample mechanical properties.[12]

The curves in Figure 3b also demonstrate the different deformation mechanisms between the UV cured samples and the uncured samples. For all the samples that did not undergo UV curing (due to either zero PI content or zero UV irradiation time), a wide plateau region appeared on their tensile stress-strain curves after the initial rapid stress increases, which is a common tensile behavior for ductile polymers (often called cold drawing) and is attributed to chain slip and alignment that occur during the deformation process. It is this slip and alignment process that allows the samples to undergo large deformation under tension. By contrast, the stresses in the cured samples continued to increase after the initial rapid increases, suggesting a different material deformation mechanism (termed strain hardening). After crosslinking, polymer chains are covalently connected to form a network structure, which largely prevents the chain slip and alignment from occurring. This strong network structure imparts increased resistance to sample deformation and thus leads to the stress positively correlated to the strain.[58]

**Effect of MAh Dosage.** The loading of MAh in MSPI synthesis affects the degree of methacrylation of SPI. The MSPI with a higher degree of methacrylation would be expected to

show a higher crosslinking density and thus higher mechanical properties after UV curing. Figure 4 presents the tensile stress-strain curves for the MSPI films synthesized with 6%, 10%, and 14% MAh. The tensile property values are summarized in Table S2. Apparently, all the samples showed a strain hardening behavior due to the crosslinked polymer network. The failure stresses and moduli of the samples increased with increasing MAh content. From 6% to 14% MAh, the stress and modulus increased from 3.57 MPa and 24.62 MPa to 7.37 MPa and 90.42 MPa, respectively, confirming the higher degree of methacrylation and higher crosslinking density at 14% MAh.[59] In the following sections, MSPI synthesized with 10% MAh was chosen as the matrix polymer to study the effects of CNF, MCNF, CNC, and MCNC on the properties of soy plastics.

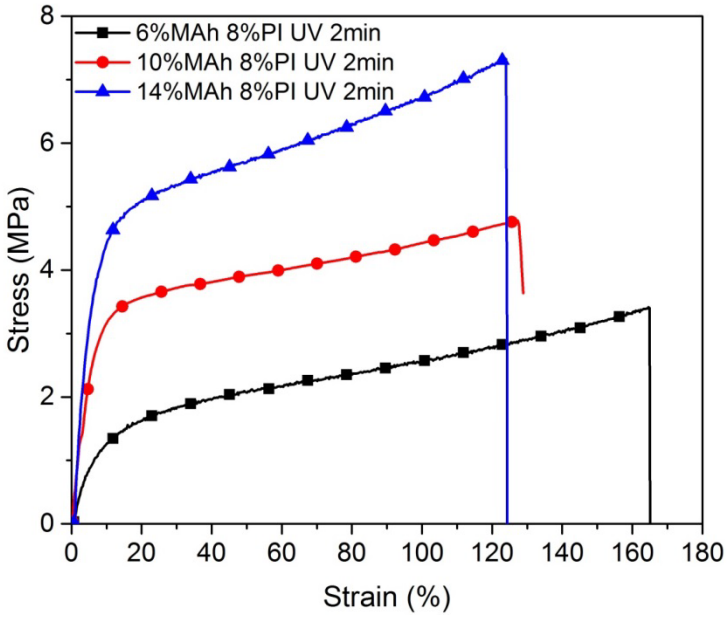


**Figure 4.** Tensile stress-strain curves of MSPI films synthesized using different contents of MAh. All samples contained 8% PI and underwent 2 min UV irradiation.

**Effects of Cellulose nanofibers on MSPI Mechanical Properties.** The reinforcing effects of CNF, MCNF, CNC, or MCNC on uncured MSPI films can be clearly seen from the stress-strain curves in Figure 5 and from the property data summarized in Table S3. Without UV curing, both

the failure stress and modulus increased significantly after the incorporation of all four types of nanofibers while the failure strain decreased as the samples became less flexible. The increases are ascribed to the strong reinforcement of the cellulose nanofillers, which originates from their high mechanical properties, high aspect ratio, and strong interfacial bonding with the MSPI matrix.[29,60] Comparing CNF (or MCNF) with CNC (or MCNC), the former showed a stronger reinforcing effect on MSPI than the latter, which can be mainly attributed to the former's higher aspect ratio. The longer length of CNF not only allows a larger stress transfer on its fiber-matrix interface but also promotes the formation of a percolation CNF network in the matrix, both leading to a higher strength and a higher modulus of the composites. CNF (or MCNF) also resulted in lower failure strains than CNC (or MCNC), a result of a stronger constraint imposed by the CNF network on material deformation and a higher likelihood of CNF fiber agglomeration. Similar results have also been reported in an earlier study where CNC and CNF were used to reinforce PEO.[29] The CNF (or MCNF) network also demonstrated its effects on the stress-strain behavior of the composites: the CNF (or MCNF) reinforced samples showed continuous increases in stress while the CNC (or MCNC) reinforced samples showed wide stress plateaus similar to neat polymer.

Methacrylation of the cellulose nanofibers also had an impact on the mechanical properties of the uncured MSPI films. As shown in Figure 5 and Table S3, the samples reinforced by methacrylated cellulose nanofibers exhibited higher failure strain than their pristine counterparts. This result may be attributed to two reasons. Firstly, the polarity of the pristine nanofibers is reduced after the methacrylation, which increases the compatibility between the nanofibers and the protein and hence reduces the likelihood of fiber agglomeration in the samples consisting of the methacrylated nanofibers.[38,61] Secondly, the samples incorporated with methacrylated nanofibers contained a higher content of PI (0.8% higher) than the samples reinforced by pristine

nanofibers. This higher content in the former samples was based on the greater need of PI for initiating a higher number of methacrylate groups. The PI used in this study is an oily liquid and therefore can function as a plasticizer in the composites that do not undergo UV curing. Therefore, the plasticization effect of the PI also contributed to the larger failure strain of the samples including the methacrylated nanofibers. The methacrylated nanofibers was also observed to lead to a lower failure stress and modulus of the composites than did the pristine nanofibers. This can be partially ascribed to the plasticizing effect of PI. It can also be caused by the decrease in cellulose nanofiber crystallinity and nanofiber length, a result of the methacrylation process.[62,63]

All the films after UV curing (Figures 5b and 5c) exhibited higher failure stresses and moduli than their uncured counterparts shown in Figure 5a, demonstrating the effect of crosslinking. Specifically, the samples consisting of CNC (or MCNC), which showed the wide stress plateaus before curing, exhibited continuous stress increases after curing, further indicating the formation of a UV-initiated network. The failure stresses and moduli of the samples containing methacrylated nanofibers were lower than those of the samples containing pristine nanofibers before the samples were cured. UV curing led to greater increases in the stress and modulus for the former than the latter, resulting in similar results between the two types of cured samples. The reason for this is that more methacrylate groups (from the methacrylated nanofibers) are available for the crosslinking reactions during the curing process and the covalent bonds between MSPI and MCNC (or MCNF) and between the nanofibers themselves can be formed after curing.

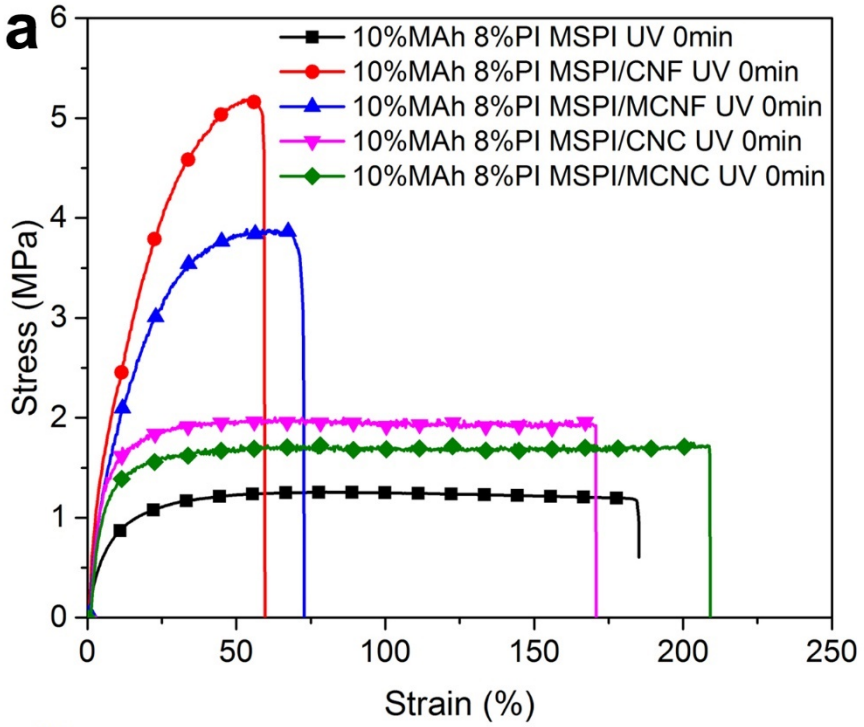
a
10%MAh 8%PI MSPI UV 0min
10%MAh 8%PI MSPI/CNF UV 0min
10%MAh 8%PI MSPI/MCNF UV 0min
10%MAh 8%PI MSPI/CNC UV 0min
10%MAh 8%PI MSPI/MCNC UV 0min
Stress (MPa)
Strain (%)
0
1
2
3
4
5
6
0
50
100
150
200
250

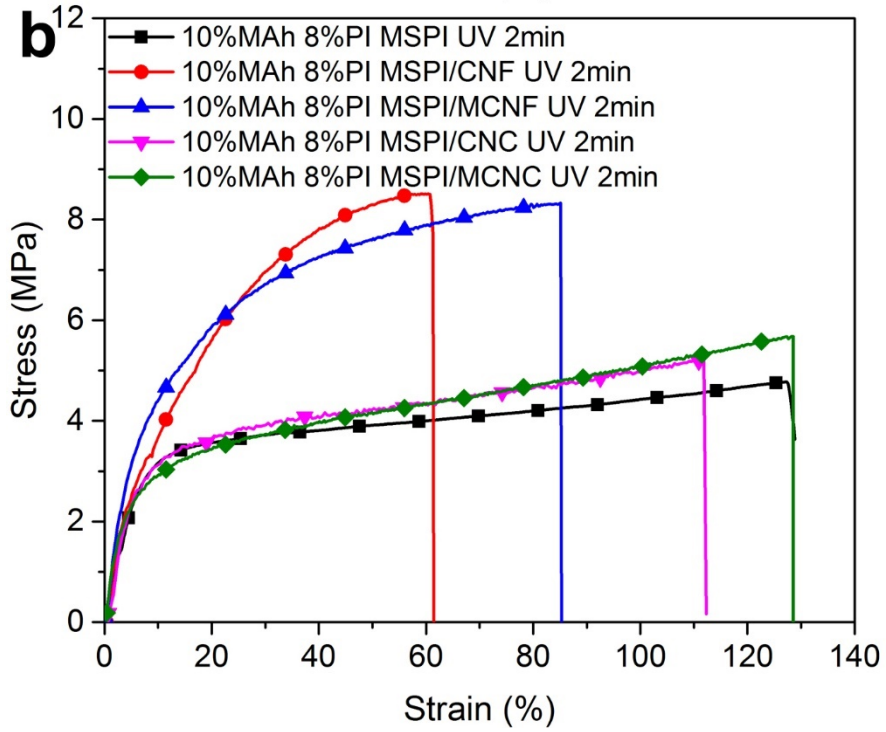
b
10%MAh 8%PI MSPI UV 2min
10%MAh 8%PI MSPI/CNF UV 2min
10%MAh 8%PI MSPI/MCNF UV 2min
10%MAh 8%PI MSPI/CNC UV 2min
10%MAh 8%PI MSPI/MCNC UV 2min
Stress (MPa)
Strain (%)
0
2
4
6
8
10
12
0
20
40
60
80
100
120
140

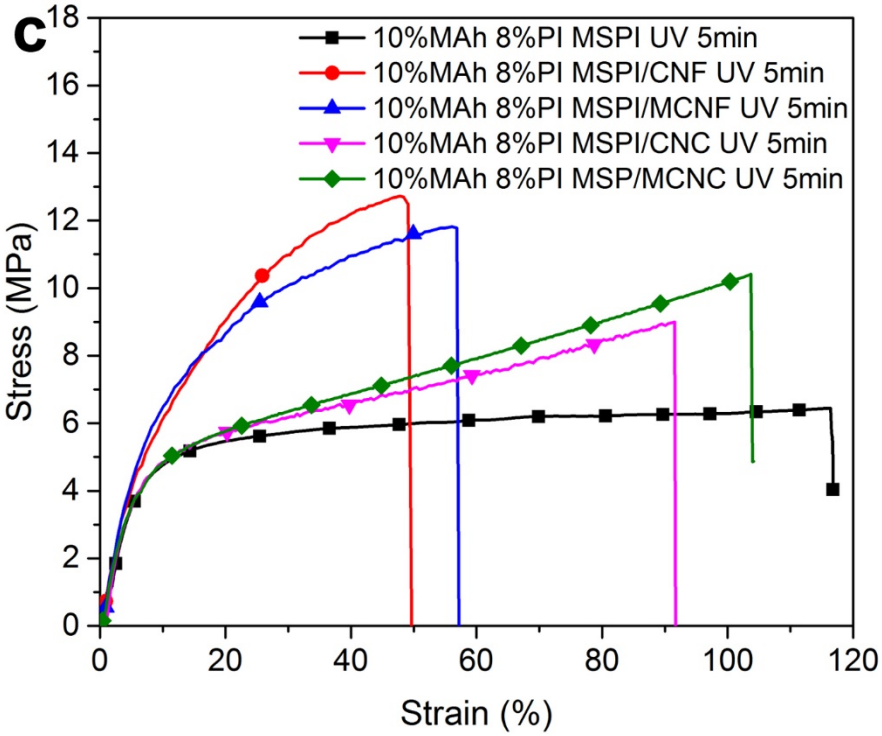


**Figure 5.** Tensile stress-strain curves of MSPI films reinforced by 10% CNF, MCNF, CNC, or MCNC. MSPI was synthesized using 10% MAh. The films were cured by UV irradiation for 0 (a), 2 (b), and 5 (c) min.

**Interaction between Cellulose Nanofibers and MSPI Matrix.** SEM imaging of sample surfaces and cross-sections, XRD, and FTIR were used to investigate the interactions between the two materials. The pure MSPI film exhibited a smooth, flat and homogeneous surface and cross-section, with the cross-section showing typical crack propagation marks (see Figures 6a and a').[18,47] The films containing CNF or MCNF clearly showed the nanofibers and their aggregates on the sample surfaces/cross-sections (see Figures 6b, b', c, and c'). However, the latter demonstrated a much lower degree of fiber aggregation than the former, indicating that the methacrylation of CNF improved the nanofiber's compatibility with MSPI. The surfaces/cross-sections of the films containing CNC or MCNC were much smoother and showed much less

microstructural features than those containing CNF or MCNF. The observed better dispersion of the cellulose nanocrystals can be attributed to their much shorter length and fewer entanglements than the nanofibrils. The methacrylation also improved CNC's compatibility with the MSPI matrix as MSPI/MCNC showed smoother surfaces/cross-sections than MSPI/CNC (see Figures 6d, d', e and e'). Especially, MSPI/MCNC showed a surface similar to that of the pure MSPI sample, suggesting the uniform dispersion of the nanocrystals and high homogeneity of the composite. The enhanced compatibility of the methacrylated cellulose nanofibers (i.e. MCNF or MCNC) can be attributed to the decreases in their polarity, crystallinity, and fiber length.[61] The results from the SEM investigation are in accordance with the discussion about the mechanical properties of the films.

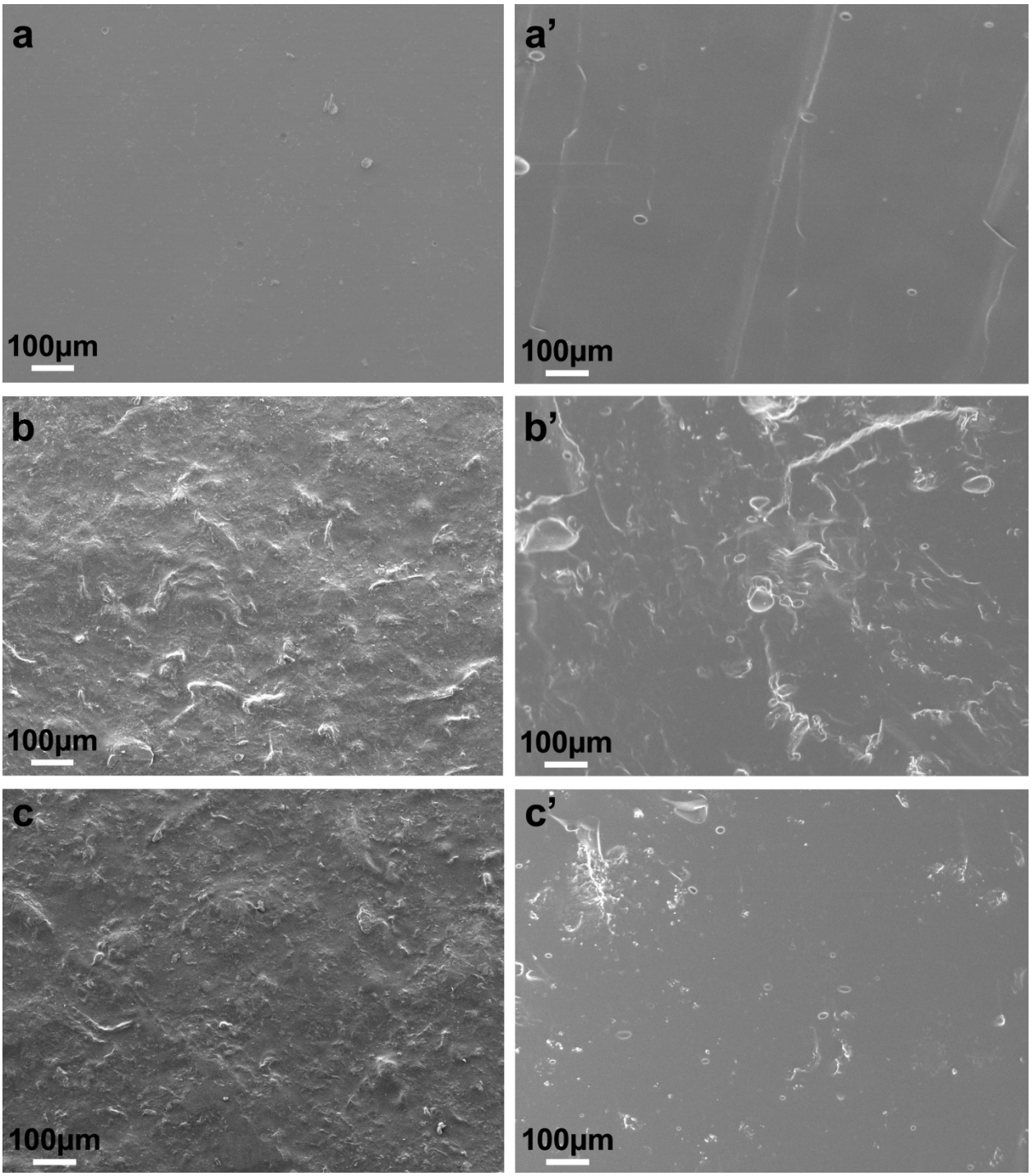
a
100μm
a'
100μm
b
100μm
b'
100μm
c
100μm
c'
100μm

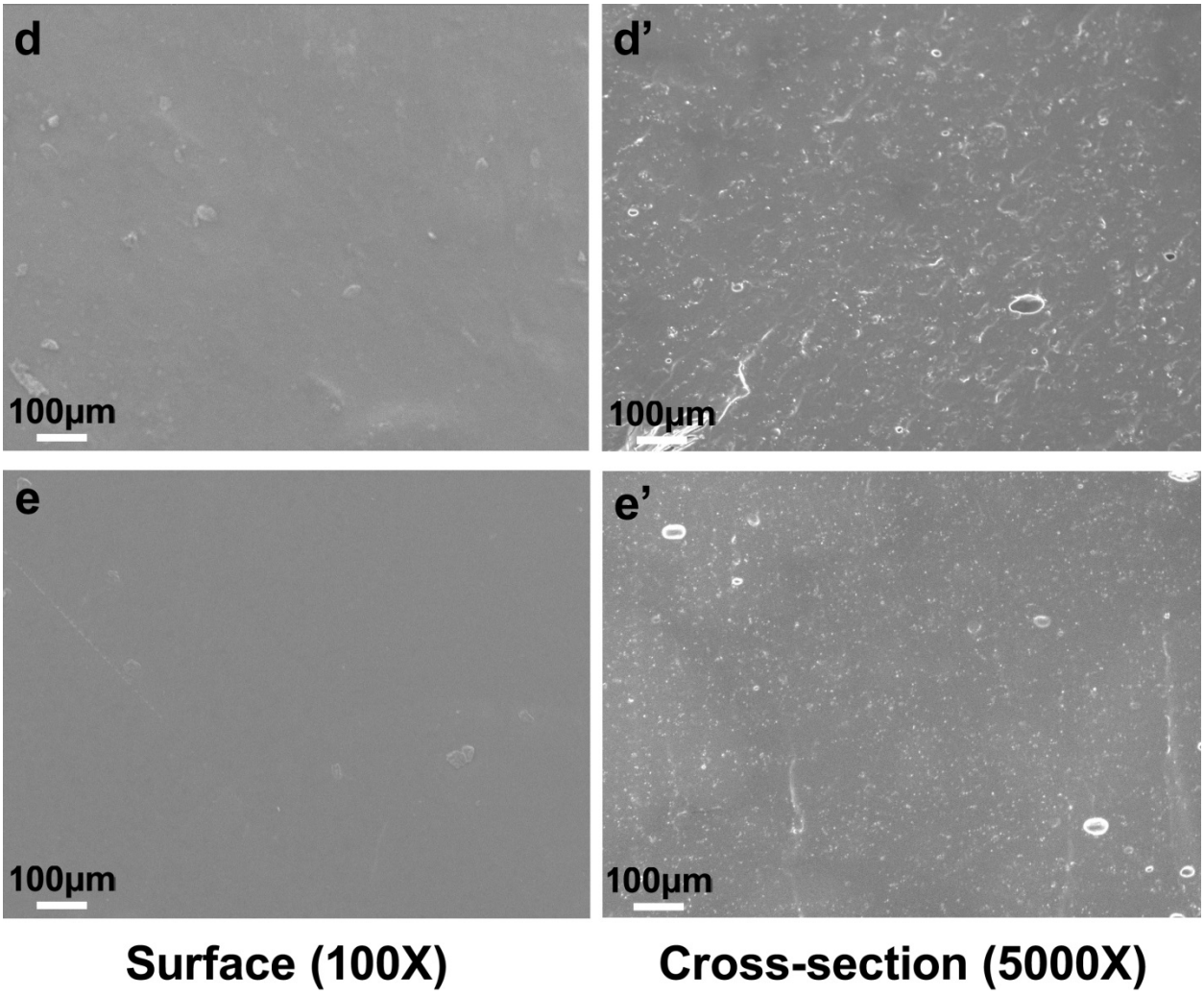


**Figure 6.** SEM images of MSPI (a, a'), MSPI/CNF (b, b'), MSPI/MCNF (c, c'), MSPI/CNC (d, d'), MSPI/MCNC (e, e') films. MSPI was synthesized using 10% MAh. The content of CNF, MCNF, CNC, or MCNC is 10% in each case. All films were cured by UV irradiation for 5 min.

XRD spectra of MSPI based films are presented in Figure 7 and their crystallinity indexes (CI) are summarized in Table S4. The alkaline-treated SPI film had the characteristic β-sheet structure of SPI at 2θ = 20.04º. After methacrylation, the β-sheet peak shifted to a higher 2θ of 21.25º and greatly broadened and weakened, implying the less ordered crystalline structure of the protein and the breakage of hydrogen bonding between its peptide chains.[18] Interestingly, the β-sheet peak

shifted back to the original 2θ and became markedly sharpened and intensified after curing, indicating the partial restoration of the crystalline structure due to the curing.[64] For all the samples containing cellulose nanofibers, a new characteristic peak at 22.36º appeared in the spectra, which was attributed to the (002) plane of cellulose I. The cured films containing CNC (or MCNC) exhibited sharper and more intense peaks at 22.36º than the ones containing CNF (or MCNF) due to CNC's higher crystallinity than CNF.[29]

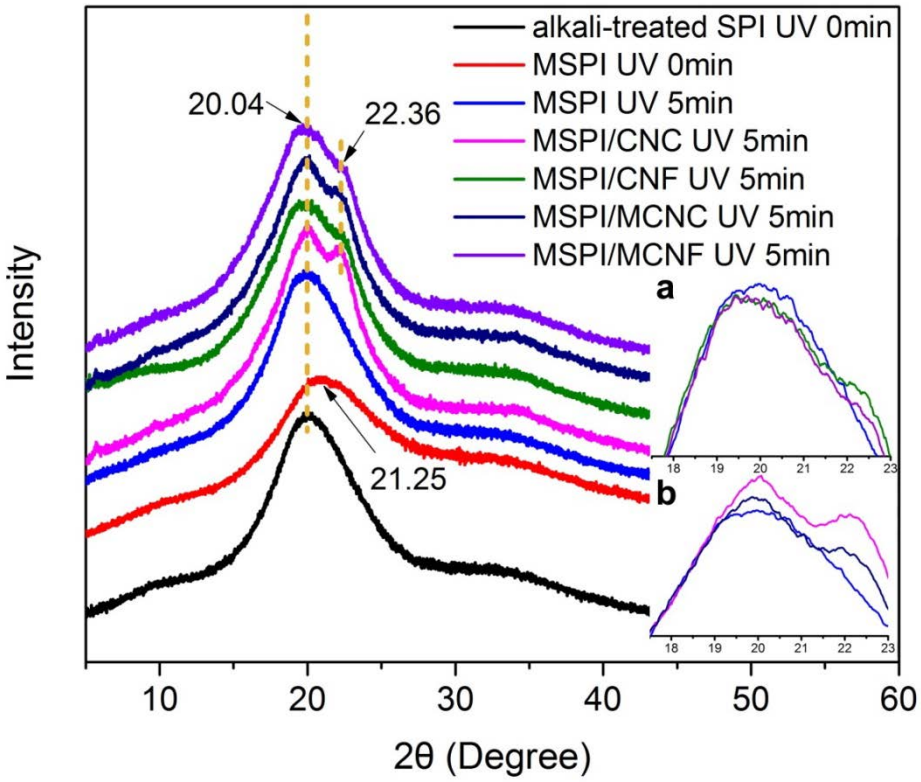


**Figure 7.** XRD spectra of alkali-treated SPI and MSPI films under different curing and reinforcement conditions. Inset a: superimposed spectra for MSPI UV 5min, MSPI/CNF UV 5 min, and MSPI/MCNF UV 5min, Inset b: superimposed spectra for MSPI UV 5min, MSPI/CNC UV 5 min, and MSPI/MCNC UV 5min. MSPI was synthesized using 10% MAh.

The β-sheet peaks of MSPI, MSPI/CNF without curing, and MSPI/MCNF cured for 5 min are compared in Inset a of Figure 7. It shows that the intensities of the peaks were slightly reduced after the incorporation of CNF. By contrast, the intensities were increased, and the peaks were sharpened after the incorporation of CNC, as shown in Inset b. These results suggest that CNF and CNC have different effects on the formation of the protein β-sheets. As discussed in the previous section, CNC and MCNC showed stronger interaction/compatibility with MSPI and were dispersed much more homogeneously in MSPI than CNF and MCNF. It is hypothesized that it is this more intimate interplay between CNC and the protein and their larger interfacial area that facilitates the formation of the β-sheets and leads to the protein's enhanced X-ray diffraction. It is also noticeable from the two insets that the intensity of the cellulose I peak (22.36º) of MCNC (or MCNF) is lower than that of its unmodified counterpart CNC (or CNF), which can be ascribed to reduced crystallinity of CNC and CNF after methacrylation.[62–65]

CIs of the films were summarized in Table S4 and the data showed a similar trend with the observation made from the diffraction peaks. The alkali-treated SPI exhibited a high CI of 60.6%. Methacrylation of the material reduced its CI to 54.3% and the value was increased to 58.5% after UV curing. The incorporation of CNC or MCNC into the material led to higher CIs than did the incorporation of CNF or MCNF.

FTIR spectra of the films are shown in Figure S1 and a detailed analysis of the spectra was provided in the Supporting Information. Due to the presence of the glycerol plasticizer in the films and the overlapping bands of amide I (soy protein) and C=C (grafted methacrylate), it is difficult to detect hydrogen bonding or crosslinking between the protein matrix and the cellulose nanofibers.

**Effects of Cellulose Nanofibers on MSPI Water Resistance.** Images of the samples after 8 hours of water immersion are shown in Figure 9. All the uncured samples (0 min) broke apart into

small pieces during the immersion test, regardless of the incorporation of CNF, MCNF, CNC, or MCNC. Therefore, the cellulose nanofibers alone cannot satisfactorily increase the water resistance of the films. Nevertheless, the films consisting of the nanofibers (especially MCNC, CNF, and MCNF) did show some degree of improvement because disintegrated pieces from these films were larger compared with those from the neat film. For the samples cured for 2 min, the neat MSPI film and the film reinforced by CNC (Figure 9a' and b') disintegrated into several large pieces while the films reinforced by CNF, MCNF, or MCNC (Figure 9c', d', and e') were able to maintain their structural integrity, indicating the strong effects of the nanofibers (especially CNF and MCNF) and methacrylation on the improvement of the film water resistance. Even for the disintegrated neat MSPI and MSPI/CNC films, 2-min UV curing still improved their water resistance, as the disintegrated pieces were much larger than those without UV curing. In addition, the fact that CNF could maintain film integrity (whereas CNC could not under the same condition) again suggests the presence of a CNF percolation network in the MSPI/CNF film.

Curing time also played a factor in sample water resistance. The samples reinforced by CNF, MCNF, or MCNC showed less swelling after 5 min curing than after 2 min curing. A longer curing time leads to a higher crosslinking density, causing a more tightly connected structure which allows less water ingression and swelling.[46,58] Moreover, comparing d' and e' reveals that the sample containing MCNF showed less swelling than the sample containing CNF, which is attributed to the strong covalent bonding between MCNF and MSPI and higher hydrophobicity of MCNF compared with CNF.

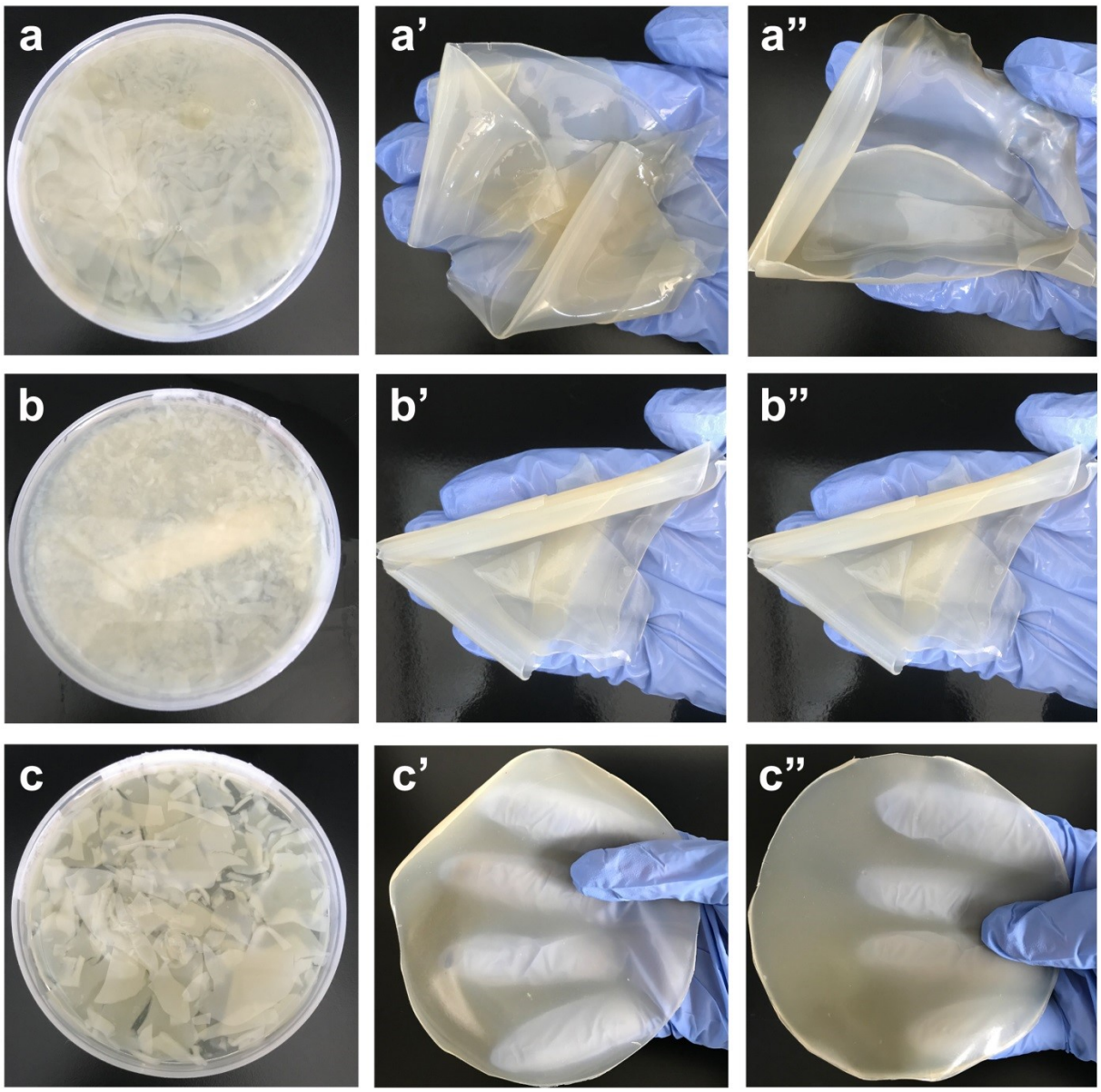
a
a'
a''
b
b'
b''
c
c'
c''

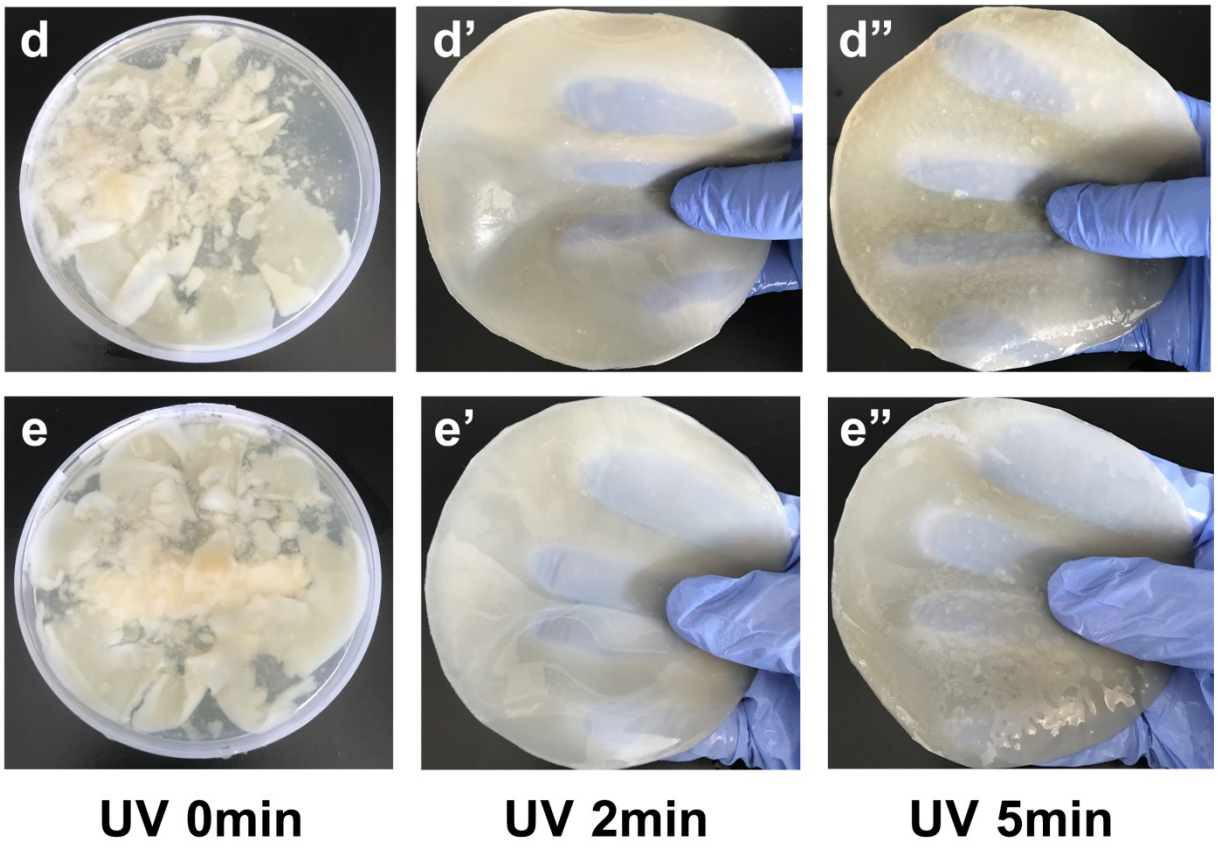


**Figure 8.** Images of MSPI (a, a', a"), MSPI/CNC (b, b', b"), MSPI/MCNC (c, c', c"), MSPI/CNF (d, d', d"), MSPI/MCNF (e, e', e") films after 8 hours of water immersion. MSPI was synthesized using 10% MAh. The content of CNF, MCNF, CNC, and MCNC is 10% in each case.

The tensile properties of the films after the water immersion were measured to further evaluate their water resistance. Figures 9 shows the stress-strain curves of six water treated films and their mechanical properties are summarized in Table S5. Compared with the tensile results for the dry films (Figure 5 and Table S3), the failure stress, failure strain, and elastic modulus of the water treated samples all decreased substantially. The decreases are understandable because the water-treated samples contained large contents of water, which functioned as a plasticizer to separate polymer chains and reduce their interactions, weakening the materials. It is also possible that some

components of the films, e.g. unreacted soy protein molecules, leached out of the samples during the immersion, further weakening the films.[50,58,59] Similar to the dry films, a longer curing time led to a higher failure stress and modulus but a lower fracture strain for the wet samples, due to the increased crosslinking density after a longer curing process. The MSPI/CNF and MSPI/MCNF wet films also exhibited higher mechanical properties than the MSPI/MCNC wet film, mirroring the trend found in the dry films. The comparison of the properties agrees with the visual observation in Figure 8, further demonstrating the advantages of CNF's long fiber length in improving the mechanical properties and water resistance of the soy protein resin.

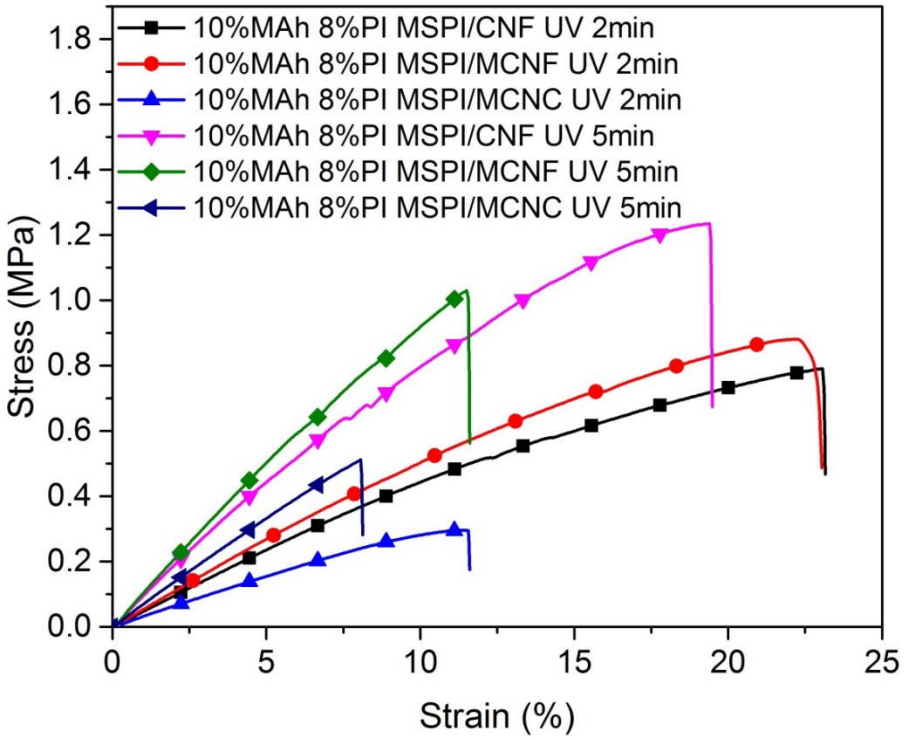


**Figure 9.** Tensile stress-strain curves of MSPI films reinforced with 10% CNF, MCNF, or MCNC after 2- or 5-min curing. The films were tested after 8 hours water immersion. MSPI was synthesized using 10% MAh. All films contain 8% PI.

**Applications in Extrusion and 3D Printing.** The developed MSPI resin can be readily adopted in traditional plastics processing and also in 3D printing after a formulation adjustment for each process. Figure 10a demonstrates the resin being extruded into plastic sheets using a HAAKE PolyLab twin-screw extruder and Figure 10b shows the resin being 3D printed into a cylindrical product using an in-house developed FDM (fused deposition modeling) 3D printer. The printed article could hold its structure and shape without collapsing due to the resin's relatively high viscosity. The article was then placed under a UV lamp to be cured into a rigid part. The formulation of the resin could be adjusted to have a lower viscosity. In this case, the resin was partially cured while being deposited using a UV laser which tracked the nozzle tip (see Figure 10c). Post-curing was followed after the printing was completed. These demonstrations show that the resin is versatile for different industrial processing methods and formulation adjustments are relatively easy, involving mainly changing the ratio of the ingredients.

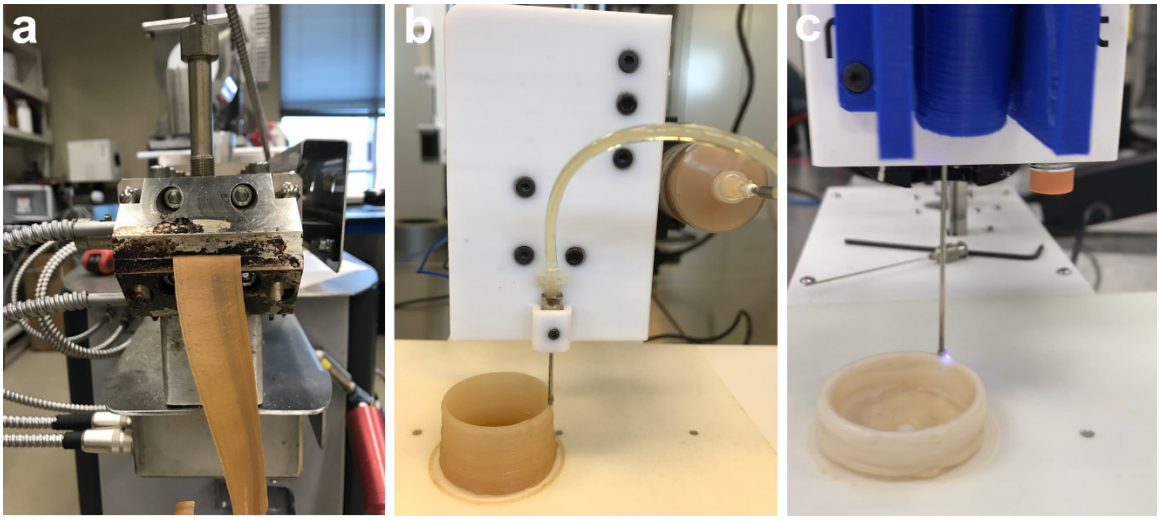


**Figure 10.** MSPI resin being processed into a sheet by (a) twin-screw extrusion and into a flowerpot by (b) 3D printing without a tracking UV laser, and (c) with a tracking UV laser.

CONCLUSION

In this study, we developed a technique that combines the advantages of UV curing and nanofiber reinforcement to obtain UV curable soy plastics that exhibit greatly enhanced mechanical properties and water resistance. Surface-modified, UV curable MSPI, MCNC, and MCNF were prepared by methacrylation of SPI, CNC, and CNF, respectively. UV exposure time and the degree of methacrylation of MSPI were shown to have significant effects on the mechanical properties and water resistance of the MSPI films. Longer exposure time and higher methacrylation degree led to higher sample tensile strength, modulus, and water resistance but lower ductility because of a higher crosslinking density of the sample. The incorporation of the cellulose nanofibers into MSPI further improved its mechanical properties and water resistance because of the superior reinforcement effect of the nanofibers and CNF's capability to form network structures in the matrix. Among the four types of the cellulose nanofibers, MCNF led to the largest increases in strength, modulus, and water resistance of the soy plastics. The synergistic effect of photo-crosslinking and cellulose nanofiber reinforcement discovered in this study provides a facile, effective method to improve the mechanical and water resistance performance of soy plastics, which can be processed using the traditional plastic molding processes and the modern 3D printing technology. This technique can potentially offer great economic and environmental benefits to society as it solves one of the most difficult issues facing current soy plastics.

## ACKNOWLEDGMENTS

The authors thank North Dakota Soybean Council for providing funding support to this project and Electron Microscopy Center NDSU for the SEM imaging service.

## REFERENCES

(1) Karan, H.; Funk, C.; Grabert, M.; Oey, M.; Hankamer, B. Green Bioplastics as Part of a Circular Bioeconomy. *Trends in plant science* **2019**, *24* (3), 237–249.
(2) Dobrucka, R. Bioplastic Packaging Materials in Circular Economy. *LogForum* **2019**, *15* (1).
(3) Galus, S.; Kadzińska, J. Gas Barrier and Wetting Properties of Whey Protein Isolate-Based Emulsion Films. *Polymer Engineering & Science* **2019**, *59* (S1), E375–E383.
(4) Hassan, B.; Chatha, S. A. S.; Hussain, A. I.; Zia, K. M.; Akhtar, N. Recent Advances on Polysaccharides, Lipids and Protein Based Edible Films and Coatings: A Review. *International Journal of Biological Macromolecules* **2018**, *109*, 1095–1107.
(5) Hu, X.; Jia, X.; Zhi, C.; Jin, Z.; Miao, M. Improving the Properties of Starch-Based Antimicrobial Composite Films Using ZnO-Chitosan Nanoparticles. *Carbohydrate polymers* **2019**, *210*, 204–209.
(6) Zhang, J.; Jiang, L.; Zhu, L.; Jane, J.; Mungara, P. Morphology and Properties of Soy Protein and Polylactide Blends. *Biomacromolecules* **2006**, *7* (5), 1551–1561. https://doi.org/10.1021/bm050888p.
(7) Zubair, M.; Ullah, A. Recent Advances in Protein Derived Bionanocomposites for Food Packaging Applications. *Critical Reviews in Food Science and Nutrition* **2020**, *60* (3), 406–434.
(8) Capezza, A. J.; Newson, W. R.; Olsson, R. T.; Hedenqvist, M. S.; Johansson, E. Advances in the Use of Protein-Based Materials: Toward Sustainable Naturally Sourced Absorbent Materials. *ACS Sustainable Chem. Eng.* **2019**, *7* (5), 4532–4547. https://doi.org/10.1021/acssuschemeng.8b05400.
(9) Reddy, M.; Mohanty, A. K.; Misra, M. Thermoplastics from Soy Protein: A Review on Processing, Blends and Composites. *J Biobased Mat Bioenergy* **2010**, *4* (4), 298–316. https://doi.org/10.1166/jbmb.2010.1112.
(10) Vieira, M. G. A.; da Silva, M. A.; dos Santos, L. O.; Beppu, M. M. Natural-Based Plasticizers and Biopolymer Films: A Review. *European Polymer Journal* **2011**, *47* (3), 254–263.
(11) Liu, B.; Jiang, L.; Liu, H.; Sun, L.; Zhang, J. Different Effects of Water and Glycerol on Morphology and Properties of Poly(Lactic Acid)/Soy Protein Concentrate Blends. *Macromolecular Materials and Engineering* **2009**, NA-NA. https://doi.org/10.1002/mame.200900224.
(12) Garrido, T.; Leceta, I.; Cabezudo, S.; Guerrero, P.; de la Caba, K. Tailoring Soy Protein Film Properties by Selecting Casting or Compression as Processing Methods. *European Polymer Journal* **2016**, *85*, 499–507.
(13) Wang, Z.; Zhou, J.; Wang, X.; Zhang, N.; Sun, X.; Ma, Z. The Effects of Ultrasonic/Microwave Assisted Treatment on the Water Vapor Barrier Properties of Soybean Protein Isolate-Based Oleic Acid/Stearic Acid Blend Edible Films. *Food Hydrocolloids* **2014**, *35*, 51–58. https://doi.org/10.1016/j.foodhyd.2013.07.006.
(14) Garrido, T.; Etxabide, A.; Leceta, I.; Cabezudo, S.; De La Caba, K.; Guerrero, P. Valorization of Soya By-Products for Sustainable Packaging. *Journal of cleaner production* **2014**, *64*, 228–233.
(15) Wihodo, M.; Moraru, C. I. Physical and Chemical Methods Used to Enhance the Structure and Mechanical Properties of Protein Films: A Review. *Journal of Food Engineering* **2013**, *114* (3), 292–302.

(16) Kumar, R.; Choudhary, V.; Mishra, S.; Varma, I. K.; Mattiason, B. Adhesives and Plastics Based on Soy Protein Products. *Industrial Crops and Products* **2002**, *16* (3), 155–172. https://doi.org/10.1016/S0926-6690(02)00007-9.
(17) Aydogdu, A.; Yildiz, E.; Ayhan, Z.; Aydogdu, Y.; Sumnu, G.; Sahin, S. Nanostructured Poly (Lactic Acid)/Soy Protein/HPMC Films by Electrospinning for Potential Applications in Food Industry. *European Polymer Journal* **2019**, *112*, 477–486.
(18) Ye, Q.; Han, Y.; Zhang, J.; Zhang, W.; Xia, C.; Li, J. Bio-Based Films with Improved Water Resistance Derived from Soy Protein Isolate and Stearic Acid via Bioconjugation. *Journal of cleaner production* **2019**, *214*, 125–131.
(19) Liu, B.; Jiang, L.; Liu, H.; Zhang, J. Synergetic Effect of Dual Compatibilizers on in Situ Formed Poly(Lactic Acid)/Soy Protein Composites. *Industrial & Engineering Chemistry Research* **2010**, *49* (14), 6399–6406. https://doi.org/10.1021/ie100218t.
(20) Chen, F.; Zhang, J. A New Approach for Morphology Control of Poly(Butylene Adipate-Co-Terephthalate) and Soy Protein Blends. *Polymer* **2009**, *50* (15), 3770–3777. https://doi.org/10.1016/j.polymer.2009.06.004.
(21) Tian, H.; Guo, G.; Fu, X.; Yao, Y.; Yuan, L.; Xiang, A. Fabrication, Properties and Applications of Soy-Protein-Based Materials: A Review. *International journal of biological macromolecules* **2018**, *120*, 475–490.
(22) Hernandez-Izquierdo, V. M.; Krochta, J. M. Thermoplastic Processing of Proteins for Film Formation—a Review. *Journal of food science* **2008**, *73* (2), R30–R39.
(23) Liu, Y.; Li, K. Development and Characterization of Adhesives from Soy Protein for Bonding Wood. *International Journal of Adhesion and Adhesives* **2007**, *27* (1), 59–67.
(24) Ma, L.; Yang, Y.; Yao, J.; Shao, Z.; Chen, X. Robust Soy Protein Films Obtained by Slight Chemical Modification of Polypeptide Chains. *Polymer Chemistry* **2013**, *4* (21), 5425–5431.
(25) González, A.; Igarzabal, C. I. A. Study of Graft Copolymerization of Soy Protein-Methyl Methacrylate: Preparation and Characterization of Grafted Films. *Journal of Polymers and the Environment* **2017**, *25* (2), 214–220.
(26) Shi, Z.; Reddy, N.; Shen, L.; Hou, X.; Yang, Y. Grafting Soyprotein Isolates with Various Methacrylates for Thermoplastic Applications. *Industrial Crops and Products* **2014**, *60*, 168–176.
(27) Deng, S.; Cheng, J.; Guo, X.; Jiang, L.; Zhang, J. Fiber Spinning of Polyacrylonitrile Grafted Soy Protein in an Ionic Liquid/DMSO Mixture Solvent. *Journal of Polymers and the Environment* **2014**, *22* (1), 17–26. https://doi.org/10.1007/s10924-013-0617-8.
(28) Coltelli, M.-B.; Wild, F.; Bugnicourt, E.; Cinelli, P.; Lindner, M.; Schmid, M.; Weckel, V.; Müller, K.; Rodriguez, P.; Staebler, A. State of the Art in the Development and Properties of Protein-Based Films and Coatings and Their Applicability to Cellulose Based Products: An Extensive Review. *Coatings* **2016**, *6* (1), 1.
(29) Xu, X.; Liu, F.; Jiang, L.; Zhu, J. Y.; Haagenson, D.; Wiesenborn, D. P. Cellulose Nanocrystals vs. Cellulose Nanofibrils: A Comparative Study on Their Microstructures and Effects as Polymer Reinforcing Agents. *ACS applied materials & interfaces* **2013**, *5* (8), 2999–3009.
(30) Rol, F.; Belgacem, M. N.; Gandini, A.; Bras, J. Recent Advances in Surface-Modified Cellulose Nanofibrils. *Progress in Polymer Science* **2019**, *88*, 241–264. https://doi.org/10.1016/j.progpolymsci.2018.09.002.

(31) Moon, R. J.; Martini, A.; Nairn, J.; Simonsen, J.; Youngblood, J. Cellulose Nanomaterials Review: Structure, Properties and Nanocomposites. *Chemical Society Reviews* **2011**, *40* (7), 3941. https://doi.org/10.1039/c0cs00108b.
(32) Lee, K.-Y.; Aitomäki, Y.; Berglund, L. A.; Oksman, K.; Bismarck, A. On the Use of Nanocellulose as Reinforcement in Polymer Matrix Composites. *Composites Science and Technology* **2014**, *105*, 15–27. https://doi.org/10.1016/j.compscitech.2014.08.032.
(33) Sinclair, A.; Jiang, L.; Bajwa, D.; Bajwa, S.; Tangpong, S.; Wang, X. Cellulose Nanofibers Produced from Various Agricultural Residues and Their Reinforcement Effects in Polymer Nanocomposites: Research Article. *Journal of Applied Polymer Science* **2018**, *135* (21), 46304. https://doi.org/10.1002/app.46304.
(34) Isogai, A.; Saito, T.; Fukuzumi, H. TEMPO-Oxidized Cellulose Nanofibers. *Nanoscale* **2011**, *3* (1), 71–85. https://doi.org/10.1039/C0NR00583E.
(35) Wang, Q. Q.; Zhu, J. Y.; Gleisner, R.; Kuster, T. A.; Baxa, U.; McNeil, S. E. Morphological Development of Cellulose Fibrils of a Bleached Eucalyptus Pulp by Mechanical Fibrillation. *Cellulose* **2012**, *19* (5), 1631–1643. https://doi.org/10.1007/s10570-012-9745-x.
(36) Chen, L.; Wang, Q.; Hirth, K.; Baez, C.; Agarwal, U. P.; Zhu, J. Y. Tailoring the Yield and Characteristics of Wood Cellulose Nanocrystals (CNC) Using Concentrated Acid Hydrolysis. *Cellulose* **2015**, *22* (3), 1753–1762. https://doi.org/10.1007/s10570-015-0615-1.
(37) Chen, L.; Zhu, J. Y.; Baez, C.; Kitin, P.; Elder, T. Highly Thermal-Stable and Functional Cellulose Nanocrystals and Nanofibrils Produced Using Fully Recyclable Organic Acids. *Green Chemistry* **2016**, *18* (13), 3835–3843. https://doi.org/10.1039/C6GC00687F.
(38) Rosilo, H.; Kontturi, E.; Seitsonen, J.; Kolehmainen, E.; Ikkala, O. Transition to Reinforced State by Percolating Domains of Intercalated Brush-Modified Cellulose Nanocrystals and Poly (Butadiene) in Cross-Linked Composites Based on Thiol–Ene Click Chemistry. *Biomacromolecules* **2013**, *14* (5), 1547–1554.
(39) Rodionova, G.; Lenes, M.; Eriksen, Ø.; Gregersen, Ø. Surface Chemical Modification of Microfibrillated Cellulose: Improvement of Barrier Properties for Packaging Applications. *Cellulose* **2011**, *18* (1), 127–134.
(40) Sethi, J.; Farooq, M.; Sain, S.; Sain, M.; Sirviö, J. A.; Illikainen, M.; Oksman, K. Water Resistant Nanopapers Prepared by Lactic Acid Modified Cellulose Nanofibers. *Cellulose* **2018**, *25* (1), 259–268.
(41) Wohlhauser, S.; Delepierre, G.; Labet, M.; Morandi, G.; Thielemans, W.; Weder, C.; Zoppe, J. O. Grafting Polymers *from* Cellulose Nanocrystals: Synthesis, Properties, and Applications. *Macromolecules* **2018**, *51* (16), 6157–6189. https://doi.org/10.1021/acs.macromol.8b00733.
(42) Zhang, S.; Xia, C.; Dong, Y.; Yan, Y.; Li, J.; Shi, S. Q.; Cai, L. Soy Protein Isolate-Based Films Reinforced by Surface Modified Cellulose Nanocrystal. *Industrial Crops and Products* **2016**, *80*, 207–213.
(43) Zheng, T.; Yu, X.; Pilla, S. Mechanical and Moisture Sensitivity of Fully Bio-Based Dialdehyde Carboxymethyl Cellulose Cross-Linked Soy Protein Isolate Films. *Carbohydrate polymers* **2017**, *157*, 1333–1340.
(44) Kang, H.; Song, X.; Wang, Z.; Zhang, W.; Zhang, S.; Li, J. High-Performance and Fully Renewable Soy Protein Isolate-Based Film from Microcrystalline Cellulose via Bio-Inspired Poly (Dopamine) Surface Modification. *ACS Sustainable Chemistry & Engineering* **2016**, *4* (8), 4354–4360.

(45) Song, W.; Xin, J.; Zhang, J. One-Pot Synthesis of Soy Protein (SP)-Poly (Acrylic Acid)(PAA) Superabsorbent Hydrogels via Facile Preparation of SP Macromonomer. *Industrial crops and products* **2017**, *100*, 117–125.
(46) Shin, H.; Olsen, B. D.; Khademhosseini, A. The Mechanical Properties and Cytotoxicity of Cell-Laden Double-Network Hydrogels Based on Photocrosslinkable Gelatin and Gellan Gum Biomacromolecules. *Biomaterials* **2012**, *33* (11), 3143–3152.
(47) Ortiz, C. M.; Salgado, P. R.; Dufresne, A.; Mauri, A. N. Microfibrillated Cellulose Addition Improved the Physicochemical and Bioactive Properties of Biodegradable Films Based on Soy Protein and Clove Essential Oil. *Food Hydrocolloids* **2018**, *79*, 416–427.
(48) Lal, S. S.; Mhaske, S. T. TEMPO-Oxidized Cellulose Nanofiber/Kafirin Protein Thin Film Crosslinked by Maillard Reaction. *Cellulose* **2019**, *26* (10), 6099–6118. https://doi.org/10.1007/s10570-019-02509-7.
(49) Zhao, S.; Wen, Y.; Wang, Z.; Kang, H.; Li, J.; Zhang, S.; Ji, Y. Preparation and Demonstration of Poly (Dopamine)-Triggered Attapulgite-Anchored Polyurethane as a High-Performance Rod-like Elastomer to Reinforce Soy Protein-Isolated Composites. *Applied Surface Science* **2018**, *442*, 537–546.
(50) Han, Y.; Yu, M.; Wang, L. Soy Protein Isolate Nanocomposites Reinforced with Nanocellulose Isolated from Licorice Residue: Water Sensitivity and Mechanical Strength. *Industrial Crops and Products* **2018**, *117*, 252–259.
(51) Hamcerencu, M.; Desbrieres, J.; Khoukh, A.; Popa, M.; Riess, G. Synthesis and Characterization of New Unsaturated Esters of Gellan Gum. *Carbohydrate Polymers* **2008**, *71* (1), 92–100.
(52) Kim, S. H.; Yeon, Y. K.; Lee, J. M.; Chao, J. R.; Lee, Y. J.; Seo, Y. B.; Sultan, M. T.; Lee, O. J.; Lee, J. S.; Yoon, S. Precisely Printable and Biocompatible Silk Fibroin Bioink for Digital Light Processing 3D Printing. *Nature communications* **2018**, *9* (1), 1–14.
(53) Zhou, Y.; Jin, Q.; Hu, X.; Zhang, Q.; Ma, T. Heavy Metal Ions and Organic Dyes Removal from Water by Cellulose Modified with Maleic Anhydride. *Journal of Materials Science* **2012**, *47* (12), 5019–5029.
(54) Naeem, M. A.; Lv, P.; Zhou, H.; Naveed, T.; Wei, Q. A Novel in Situ Self-Assembling Fabrication Method for Bacterial Cellulose-Electrospun Nanofiber Hybrid Structures. *Polymers* **2018**, *10* (7), 712.
(55) Sahlin, K.; Forsgren, L.; Moberg, T.; Bernin, D.; Rigdahl, M.; Westman, G. Surface Treatment of Cellulose Nanocrystals (CNC): Effects on Dispersion Rheology. *Cellulose* **2018**, *25* (1), 331–345.
(56) Kobe, R.; Iwamoto, S.; Endo, T.; Yoshitani, K.; Teramoto, Y. Stretchable Composite Hydrogels Incorporating Modified Cellulose Nanofiber with Dispersibility and Polymerizability: Mechanical Property Control and Nanofiber Orientation. *Polymer* **2016**, *97*, 480–486.
(57) Cheng, X.; Qin, J.; Wang, X.; Zha, Q.; Yao, W.; Fu, S.; Tang, R. Acid-Degradable Lactobionic Acid-Modified Soy Protein Nanogels Crosslinked by Ortho Ester Linkage for Efficient Antitumor in Vivo. *European Journal of Pharmaceutics and Biopharmaceutics* **2018**, *128*, 247–258.
(58) Dong, F.; Maganty, S.; Meschter, S. J.; Cho, J. Effects of Curing Conditions on Structural Evolution and Mechanical Properties of UV-Curable Polyurethane Acrylate Coatings. *Progress in Organic Coatings* **2018**, *114*, 58–67.

(59) Teong, B.; Wu, S.-C.; Chang, C.-M.; Chen, J.-W.; Chen, H.-T.; Chen, C.-H.; Chang, J.-K.; Ho, M.-L. The Stiffness of a Crosslinked Hyaluronan Hydrogel Affects Its Chondro-Induction Activity on HADSCs. *Journal of Biomedical Materials Research Part B: Applied Biomaterials* **2018**, *106* (2), 808–816.
(60) Salari, M.; Khiabani, M. S.; Mokarram, R. R.; Ghanbarzadeh, B.; Kafil, H. S. Development and Evaluation of Chitosan Based Active Nanocomposite Films Containing Bacterial Cellulose Nanocrystals and Silver Nanoparticles. *Food Hydrocolloids* **2018**, *84*, 414–423.
(61) Ghadikolaei, S. S.; Omrani, A.; Ehsani, M. Influences of Modified Bacterial Cellulose Nanofibers (BCNs) on Structural, Thermophysical, Optical, and Barrier Properties of Poly Ethylene-Co-Vinyl Acetate (EVA) Nanocomposite. *International journal of biological macromolecules* **2018**, *115*, 266–272.
(62) Cetin, N. S.; Tingaut, P.; Özmen, N.; Henry, N.; Harper, D.; Dadmun, M.; Sebe, G. Acetylation of Cellulose Nanowhiskers with Vinyl Acetate under Moderate Conditions. *Macromolecular bioscience* **2009**, *9* (10), 997–1003.
(63) Li, W.; Wang, S.; Wang, W.; Qin, C.; Wu, M. Facile Preparation of Reactive Hydrophobic Cellulose Nanofibril Film for Reducing Water Vapor Permeability (WVP) in Packaging Applications. *Cellulose* **2019**, *26* (5), 3271–3284.
(64) Kang, H.; Wang, Z.; Wang, Y.; Zhao, S.; Zhang, S.; Li, J. Development of Mainly Plant Protein-Derived Plywood Bioadhesives via Soy Protein Isolate Fiber Self-Reinforced Soybean Meal Composites. *Industrial crops and products* **2019**, *133*, 10–17.
(65) Zhao, S.; Xing, F.; Wang, Z.; Kang, H.; Zhang, S.; Li, J. High Bonding Strength and Boiling Water Resistance of Soy Protein-Based Adhesives via Organosilicon–Acrylate Microemulsion and Epoxy Synergistic Interfacial Enhancement. *Journal of Applied Polymer Science* **2018**, *135* (16), 46061.

Synopsis

Mechanical properties and water resistance of soy based plastics were substantially improved through UV curing and cellulose nanofiber reinforcement.

TOC